Improved Modeling of the Effects of Thermal Residual Stresses on Single Fiber Pull-Out Problem

Young Suk Chai*, Byung Sun Choi
School of Mechanical Engineering, Yeungnam University, Kyungbuk 712-749, Korea
Kyung Jun Yang
Gates Korea Co., Daegu 711-855, Korea

The single fiber pull-out technique has been commonly used to characterize the mechanical behavior of fiber/matrix interface in fiber reinforced composite materials. In this study, an improved analysis considering the effect of thermal residual stresses in both radial and axial directions is developed for the single fiber pull-out test. It is found to have the pronounced effects on the stress transfer properties across the interface and the interfacial debonding behavior.

Key Words : Single Fiber Pull-Out Test, Interfacial Debonding, Thermal Residual Stress

1. Introduction

Structural reliability of composite materials can be strongly affected by the fracture properties of the interface between fiber and matrix (Gao, 1988; Hutchinson, 1990). Recently, there is much interest on the debonding and frictional sliding behavior along the interfaces in composites. The stress transfer between fiber and matrix across the interface is an important feature in fibrous composites for application to engineering technology. In the bonded region, the elastic stress transfer at the interface is determined. And significant is the stress transfer by Coulomb friction after the interface bond failure. The load bearing capacity of composites depends on the efficiency of stress transfer at interfaces, controlled by the mechanical properties of fiber and matrix and by the nature of bonding as well.

It is reported that the frictional sliding of fibers along the interface is one of the main toughening mechanisms that occur in the crack-wake-bridging zone (Gao, 1988; Hutchinson, 1990). Thus progressive debonding and frictional sliding at the interface become of fundamental interest in investigation. Single fiber pull-out techniques have been used to characterize the behavior of the interface. Initial and maximum debond stresses as well as frictional pull-out stresses can be determined with load-displacement curve from experiments. Analytical models have also been developed to provide the theoretical basis for experimental determination of the interfacial properties (Zhou, 1993a; Zhou, 1993b; Zhou, 1995).

On a single fiber moving pulled and/or pushed, a push-back phenomenon resulting in a reseating load drop was first reported by Jero and Kerans (1991) for fiber push-out. This was also confirmed by Carter et al. (1991) using a fiber pull-out test. The phenomenon of a fiber being pushed back to the original position indirectly showed that the composites have rough interface in the debonded region. Kerans and Parthasarathy (1991) included the effects of interface roughness and residual axial strain in the fiber to predict the load-displacement behavior. Their model may be appropriate for the case of relatively larger sliding displacements. In addition in many crack bridg-

* Corresponding Author,
E-mail : yschai@yu.ac.kr
TEL : +82-53-810-2464 ; **FAX** : +82-53-813-3703
School of Mechanical Engineering, Yeungnam University, #214-1, Dae-dong, Gyongsan, Kyungbuk 712-749, Korea. (Manuscript **Received** April 1, 2000; **Revised** April 12, 2001)

ing problems, since sliding displacements are small, the model is extended to include the effects of interfacial roughness by introducing a friction parameter (Parthasarathy et al, 1994a). There are other studies considering the various factors affecting single fiber pull-out and push-out phenomenon analytically and experimentally (Parthasarathy et al, 1994b; Mackin, 1992a; Mackin, 1992b; Liu, 1994; Liu, 1995; Stupkiewicz, 1996).

The present work describes an improved single fiber pull-out model in consideration of thermal residual stresses in both radial and axial directions. Most of existing analyses consider the thermal residual stress in the radial direction, arising from the mismatch of the coefficients of thermal expansion between two constituents along the interface. While previous works (Kerans, 1991; Parthasarathy et al, 1994a; Stupkiewicz, 1996) have suggested some relevant models with the interface roughness and thermal residual stresses in both directions, no effort has been made to account for the effect of the thermal residual stress in the axial direction which may affects the stress distribution in the bonded region. The interface is assumed to be initially perfectly bonded, and then partially debonded and finally completely debonded as the loads increase. A full range of loading and interfacial bond conditions, in comparison with earlier works (Liu, 1994; Liu, 1995), are considered in this paper to characterize the progressive debonding and frictional sliding behaviors during the fiber pull-out process.

Shear-lag models are generally used for modeling the fiber-matrix system and for identification of interface properties. The effect of thermal residual stress in the axial direction on the stress distribution in bonded region is rigorously considered. The axial and shear stress distributions (stress transfer properties) and the interfacial debonding behavior, stress required for further debonding, are investigated. As results, the stress distributions in bonded region are significantly affected by the presence of the thermal residual stress in the axial direction. The distribution of interfacial shear stress in bonded region suggests a possibility of two-way debonding. It is also confirmed that thermal residual stresses affect the stress transfer properties across the interface and the interfacial debonding behavior.

2. Theoretical Analysis

The geometry of a composite cylindrical model for single fiber pull-out test is depicted in Fig. 1. A system of cylindrical coordinate (r, θ, z) is selected such that the z-axis corresponds to the axis of a fiber and r is the distance from the fiber axis. L is the whole embedded axial length, and in which l is the debonded length. A fiber of radius a is located in the center of the matrix cylinder of radius b. The matrix is fixed at the bottom end $(z=L)$ and a tensile stress, σ, is applied to a fiber end $(z=0)$. The mode of deformation is axisymmetric so that all the stress and displacement components are independent of the circumferential direction θ. It is assumed that the axial stress components in both fiber and matrix are independent of the radial coordinate as in previous studies (Liu et al., 1994; Liu et al,, 1995).

2.1 Basic equations

The equilibrium of fiber, matrix and interface requires

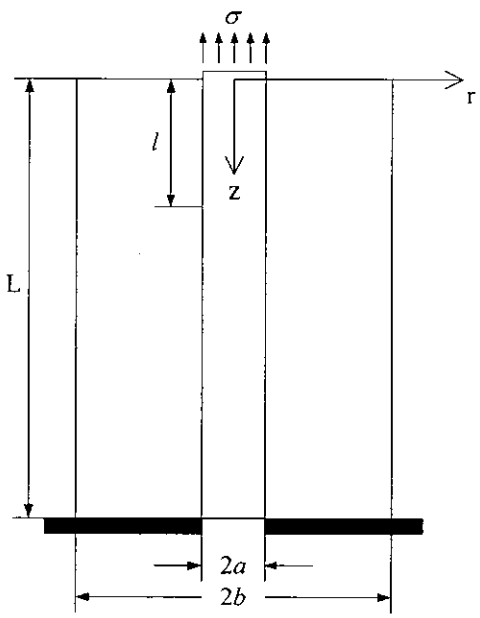

Fig. 1 Schematic of the single fiber pull-out model

$$\sigma_f^z(z)+\frac{1}{\gamma}\sigma_m^z(z)=\sigma \tag{1}$$

$$\frac{d\sigma_f^z(z)}{dz}=-\frac{1}{\gamma}\frac{d\sigma_m^z(z)}{dz}=-\frac{2}{a}\tau(z) \tag{2}$$

$$\frac{\partial\sigma_m^z(z)}{\partial z}+\frac{\partial\tau_m^{rz}(r,\ z)}{\partial r}+\frac{\tau_m^{rz}(r,\ z)}{r}=0 \tag{3}$$

where $\gamma=\frac{a^2}{b^2-a^2}$ and $\tau(z)$ is the interfacial shear stress, defined as $\tau(z)=\tau_m^{rz}(a,\ z)$. Assuming the fiber and matrix as isotropic, the stress-strain relationships are given by

$$\varepsilon_f^\theta(r,\ z)=\frac{1}{E_f}[\sigma_f^\theta(r,\ z)-\nu_f\{\sigma_f^r(r,\ z)+\sigma_f^z(z)\}]+\alpha_f\Delta T \tag{4}$$

$$\varepsilon_f^z(r,\ z)=\frac{1}{E_f}[\sigma_f^z(z)-\nu_f\{\sigma_f^r(r,\ z)+\sigma_f^\theta(r,\ z)\}]+\alpha_f\Delta T \tag{5}$$

$$\varepsilon_m^\theta(r,\ z)=\frac{1}{E_m}[\sigma_m^\theta(r,\ z)-\nu_m\{\sigma_m^r(r,\ z)+\sigma_m^z(z)\}]+\alpha_m\Delta T \tag{6}$$

$$\varepsilon_m^z(r,\ z)=\frac{1}{E_m}[\sigma_m^z(z)-\nu_m\{\sigma_m^r(r,\ z)+\sigma_m^\theta(r,\ z)\}]+\alpha_m\Delta T \tag{7}$$

From Eqs. (2) and (3), the shear stress distribution in the matrix is expressed in terms of the interfacial shear stress, $\tau(z)$

$$\tau_m^{rz}(r,\ z)=\frac{\gamma(b^2-r^2)}{ar}\tau(z) \tag{8}$$

2.2 Stresses in the debonded region ($0<z<l$)

In the debonded region, frictional slip occurs along the interface. The interfacial shear stress $\tau(z)$ is governed by Coulomb friction:

$$\tau(z)=\mu q(z) \tag{9}$$

where μ is the friction coefficient and $q(z)$ is the interfacial (compressive) radial stress represented by

$$\tau(z)=-\mu[q_o+q_a(z)] \tag{10}$$

where q_o is the thermal residual stress in the radial direction and $q_a(z)$ is the term caused by the Poisson's effect. Residual stress in the radial direction between the fiber and matrix can be derived by using the contact condition during sliding, $u_f^r(a,\ z)=u_m^r(a,\ z)$, so that the continuity of circumferential strains at the interface, $\varepsilon_f^\theta(a,\ z)=\varepsilon_m^\theta(a,\ z)$, holds from the strain-displacement relationship ($\varepsilon^\theta=\frac{u^r}{r}$). Applying $\sigma_f^\theta(a,\ z)=q_o$, $\sigma_f^r(a,\ z)=q_o$, and $\sigma_f^z(a,\ z)=0$ in Eq. (4) and $\sigma_m^\theta(a,\ z)=-(1+2\gamma)q_o$, $\sigma_m^r(a,\ z)=q_o$, and $\sigma_m^z(a,\ z)=0$ in Eq. (6) reveals

$$q_0=\frac{E_m(\alpha_m-\alpha_f)\Delta T}{\alpha(1-\nu_f)+(1+2\gamma+\nu_m)} \tag{11}$$

where α_f (α_m) is the thermal expansion coefficient of the fiber (matrix), $\alpha=\frac{E_m}{E_f}$, and ΔT is the temperature change. $q_a(z)$ caused by the Poisson's effect is also obtained from

$$q_a(z)=k_1\sigma_f^z(z)-k_2\sigma \tag{12}$$

where $k_1=\frac{\alpha\nu_f+\gamma\nu_m}{\alpha(1-\nu_f)+(1+2\gamma+\nu_m)}$ (13)

$$k_2=\frac{\gamma\nu_m}{\alpha(1-\nu_f)+(1+2\gamma+\nu_m)} \tag{14}$$

The differential equation for axial fiber stress is obtained by combining Eqs. (2), (9), and (10) as follows

$$\frac{d\sigma_f^z(z)}{dz}=-\frac{2\mu}{a}[q_o+q_a(z)] \tag{15}$$

Inserting Eqs. (11) and (12) into Eq. (15) and applying the stress boundary condition $\sigma_f^z(0)=\sigma$, the resulting solution of axial fiber stress is

$$\sigma_f^z(z)=\sigma-\omega(\bar{\sigma}-\sigma)(e^{\lambda z}-1) \tag{16}$$

where $\lambda=\frac{2\mu k_1}{a}$, $\omega=\frac{1}{k_1}(k_1-k_2)$, and

$$\bar{\sigma}=-\frac{q_0}{k_1-k_2}.$$

The stress at the debond front is obtained from $\sigma_f^z(z)$ in Eq. (16);

$$\sigma_f^l=\sigma-\omega(\bar{\sigma}-\sigma)(e^{\lambda l}-1) \tag{17}$$

From the solution of axial fiber stress $\sigma_f^z(z)$, the corresponding matrix axial stress $\sigma_m^z(z)$, and shear stress in matrix $\tau_m^{rz}(z)$ are obtained as

$$\sigma_m^z(z)=\gamma\omega(\bar{\sigma}-\sigma)(e^{\lambda z}-1) \tag{18}$$

$$\tau_m^{rz}(r,\ z)=\frac{\gamma(b^2-r^2)}{2r}\lambda\omega(\bar{\sigma}-\sigma)e^{\lambda z} \tag{19}$$

Initial frictional pull-out stress (σ_{ifr}) at the onset of complete debonding of the fiber can be determined from $\sigma_f^l=0$ when $l=L$

$$\sigma_{ifr}=\frac{\omega\bar{\sigma}(e^{\lambda L}-1)}{1+\omega(e^{\lambda L}-1)} \tag{20}$$

which is equivalent to the previous result (Liu et al., 1995).

2.3 Stresses in the bonded region ($l<z<L$)

In the bonded region, so as for no slip condition at interface, $u_m^z(a, z)=u_f^z(a, z)$ to be satisfied, the shear stress in the matrix is,

$$\tau_m^{rz}(r, z)=G\gamma_m^{rz(r,z)}=\frac{E_m}{2(1+\nu_m)}\left(\frac{\partial u_m{}^r(r, z)}{\partial z}+\frac{\partial u_m^z(r, z)}{\partial r}\right) \quad (21)$$

In the second equation of Eq. (21), the first term may be ignored compared to the second. From Eqs. (8) and (21)

$$\frac{\partial u_m^z(r, z)}{\partial r}=\frac{2(1+\nu_m)}{E_m}\frac{\gamma}{a}\frac{b^2-r^2}{r}\tau(z) \quad (22)$$

After first integrating Eq. (22), and then differentiating it with respect to z, using the no slip condition at the interface results in

$$\frac{d\tau(z)}{dz}=\frac{aE_m}{(1+\nu_m)}\frac{1}{2\gamma b^2\ln\frac{b}{a}-a^2}[\varepsilon_m^z(b, z)-\varepsilon_f^z(a, z)] \quad (23)$$

The differential equation for axial fiber stress is derived from Eqs. (1), (2), (5), (7), and (23)

$$\frac{d^2\sigma_f^z(z)}{dz^2}-\eta_1\sigma_f^z(z)=-\eta_1\eta_2\sigma-\eta_1\eta_3\sigma_o-\eta_1\eta_4 q_o \quad (24)$$

where

$$\eta_1=\frac{2}{(1+\nu_m)}\frac{(a+\gamma)-2k_1(a\nu_f+\gamma\nu_m)}{2\gamma b^2\ln\frac{b}{a}-a^2} \quad (25)$$

$$\eta_2=\frac{\gamma(1-2k_1\nu_m)}{(a+\gamma)-2k_1(a\nu_f+\gamma\nu_m)} \quad (26)$$

$$\eta_3=\frac{1}{(a+\gamma)-2k_1(a\nu_f+\gamma\nu_m)} \quad (27)$$

$$\eta_4=\frac{2(a\nu_f+\gamma\nu_m)}{(a+\gamma)-2k_1(a\nu_f+\gamma\nu_m)} \quad (28)$$

$$\sigma_o=E_m(\alpha_m-\alpha_f)\Delta T \quad (29)$$

The resulting equation of the axial stress in the bonded region subjected to the boundary condition $\sigma_f^z(l)=\sigma_f^l$ and $\sigma_f^z(L)=0$ yields

$$\sigma_f^z(z)=\frac{1}{\sinh\sqrt{\eta_1}(L-l)}[(\sigma_f^l-\eta_2\sigma-\sigma_r)\sinh\sqrt{\eta_1}(L-z)-(\eta_2\sigma+\sigma_r)\sinh\sqrt{\eta_1}(z-l)]+\eta_2\sigma+\sigma_r \quad (30)$$

where $\sigma_f^z(l)=\sigma_f^l$ is evaluated from Eq. (17) using the continuity condition of axial stress and the term, $\sigma_r=\eta_3\sigma_o+\eta_4 q_o$, is the contribution of axial and radial thermal residual stresses.

The corresponding matrix axial stress, $\sigma_m^z(z)$, and shear stress in matrix, $\tau_m^{rz}(z)$, in the bonded region are obtained by the equilibrium consideration aforementioned

$$\sigma_m^z(z)=[(1-\eta_2)\sigma-\sigma_r]\gamma-\frac{\gamma}{\sinh\sqrt{\eta_1}(L-l)}[(\sigma_f^l-\eta_2\sigma-\sigma_r)\sinh\sqrt{\eta_1}(L-z)-(\eta_2\sigma+\sigma_r)\sinh\sqrt{\eta_1}(z-l)] \quad (31)$$

$$\tau_m^{rz}(z)=\frac{\gamma(b^2-r^2)}{2r}\frac{\sqrt{\eta_1}}{\sinh\sqrt{\eta_1}(L-l)}[(\sigma_f^l-\eta_2\sigma-\sigma_r)\cosh\sqrt{\eta_1}(L-z)+(\eta_2\sigma+\sigma_r)\cosh\sqrt{\eta_1}(z-l)] \quad (32)$$

2.4 Interfacial debonding criterion

Interfacial debonding criterion is derived from Griffith energy balance equation as the rate change of the total elastic energy,

$$G_c=\frac{\partial U_t}{\partial(2\pi a l)} \quad (33)$$

The total elastic strain energy may be obtained as

$$U_t=\frac{1}{2E_f}\int_0^L\int_0^a[(\sigma_f^z)^2+(\sigma_f^r)^2+(\sigma_f^\theta)^2-2\nu_f(\sigma_f^z\sigma_f^r+\sigma_f^z\sigma_f^\theta+\sigma_f^\theta\sigma_f^r)]2\pi r dr dz+\frac{1}{2E_m}\int_0^L\int_a^b[(\sigma_m^z)^2+(\sigma_m^r)^2+(\sigma_m^\theta)^2-2\nu_m(\sigma_m^z\sigma_m^r+\sigma_m^z\sigma_m^\theta+\sigma_m^\theta\sigma_m^r)+2(1+\nu_m)(\tau_m^{rz})^2]2\pi r dr dz \quad (34)$$

The axial and shear components of stresses in the debonded and bonded regions are given in Eqs. (16), (18), (19), (30), (31), and (32). The radial and circumferential components of stresses are solved using the continuity conditions at the interface:

$$\sigma_f^r=\sigma_f^\theta=q(z) \quad (35)$$

$$\sigma_m^r=\gamma\left(\frac{b^2-r^2}{r^2}\right)q(z) \quad (36)$$

$$\sigma_m^\theta=-\gamma\left(\frac{b^2+r^2}{r^2}\right)q(z) \quad (37)$$

where $q(z)$ is the interfacial pressure which is defined independently and is easily derived from the stress fields.

After inserting proper stress fields, the energy

balance equation for fiber-matrix interfacial debonding criterion in Eq. (34) becomes

$$2\pi a G_c = m_1\sigma^2 + m_2(\bar{\sigma}-\sigma)\sigma + m_3(\bar{\sigma}-\sigma)^2 + m_4\sigma + m_5(\bar{\sigma}-\sigma) + m_6 \quad (38)$$

where the coefficients m_i's are functions of material properties and geometric factors which could be derived numerically in Appendix. Rearrangement of Eq. (38) gives the remote stress, σ, applied to the fiber for further debond propagation

$$\sigma = \frac{1}{2\bar{m}_1}[-(\bar{m}_2\bar{\sigma}+\bar{m}_3) + \sqrt{\bar{m}_4\,\bar{\sigma}^2 + \bar{m}_5\,\bar{\sigma} + \bar{m}_6 + 8\pi a\bar{m}_1 G_c}] \quad (39)$$

in which further details of the coefficients $\bar{m}_i$'s are also given in Appendix.

3. Results and Discussions

To illustrate the effects of the thermal residual stresses on the fiber pull-out problem, specific analyses were conducted for a model of steel-epoxy rod system. The basic physical and mechanical properties of the composites are in Table 1. In order to account for the effect of axial thermal residual stress, σ_o, on the stress distribution, the variation of the axial fiber stress $\sigma_f^z(z)$ and interfacial shear stress $\tau(z)$ are plotted as a function of the axial distance, z, in Fig. 2 and Fig. 3, respectively. Three different types of interfacial bond conditions, namely fully bonded, partially debonded and fully unbonded cases are examined. The debond length in the partially debonded case is determined from the debonding criterion in Eq. (39) for a given applied stress and fiber length. The general trend of the stress distribution is different between the different

Table 1 Material properties and geometrical factors

Fiber	Young's modulus E_f (GPa)	210
	Poisson's ratio ν_f	0.25
	Radius $a(mm)$	2.5
	Thermal expansion coefficient $\alpha_f^T(10^{-6}/℃)$	12
Matrix	Young's modulus $E_m(GPa)$	3
	Poisson's ratio ν_m	0.4
	Radius $b(mm)$	10
	Thermal expansion coefficient $\alpha_m^T(10^{-6}/℃)$	65
Interface	Axial length $L(mm)$	50
	Coefficient of friction μ	0.5
	Temperature change $\Delta T(℃)$	−100
	Fracture toughness $G_c(J/m^2)$	20

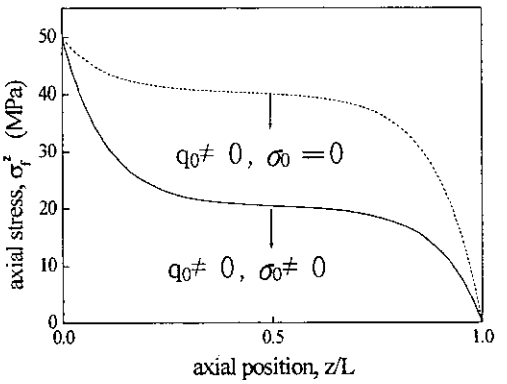

(a) Fully bonded

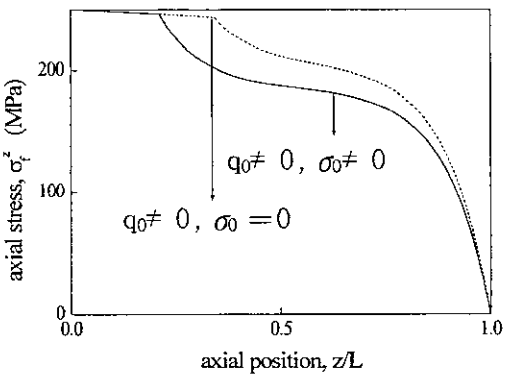

(b) Partially bonded

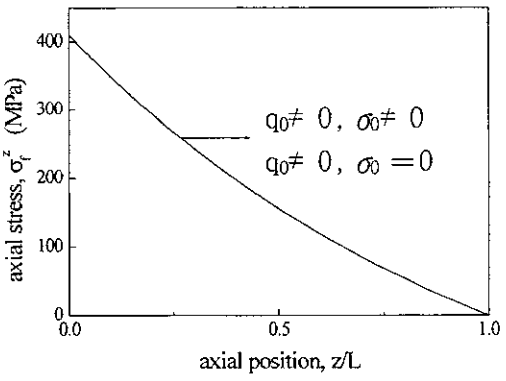

(c) Fully unbonded

Fig. 2 Axial fiber stress distribution

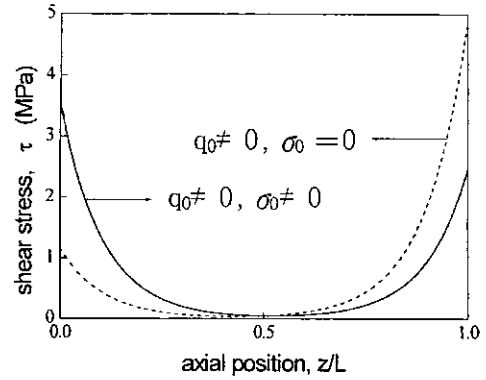

(a) Fully bonded

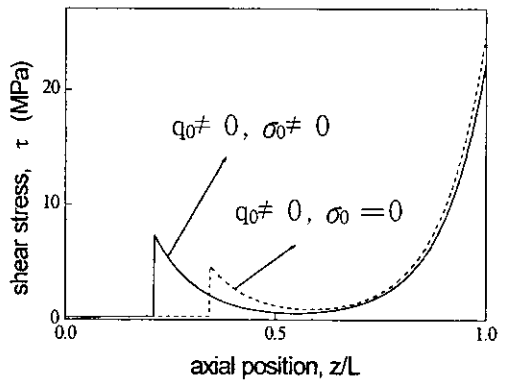

(b) Partially bonded

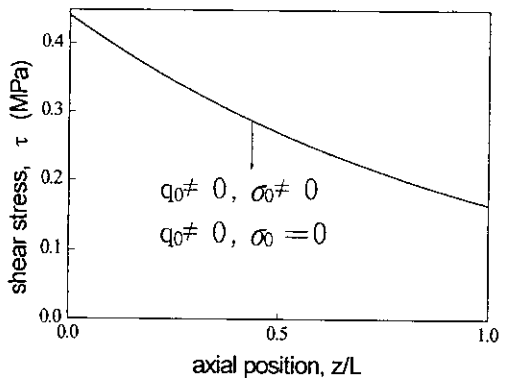

(c) Fully unbonded

Fig. 3 Interfacial shear stress distribution

interfacial bond conditions. In the bonded region (Fig. 2(a)), the axial fiber stress decreases from the loaded end ($z=0$) towards the bottom end ($z=L$) after showing a plateau region along the fiber length. The amount of the axial fiber stress was much affected by the presence of axial thermal residual stress. The result shows that the

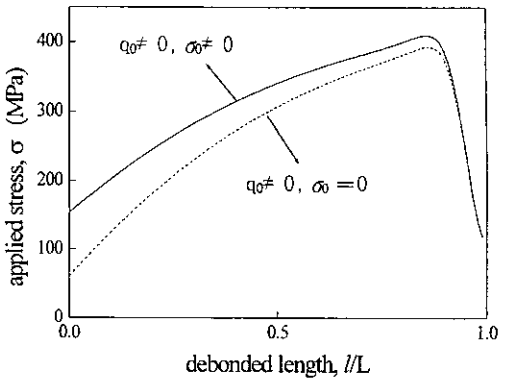

Fig. 4 Applied stress required for further debonding

amount of axial fiber stress in bonded region decreases with the axial thermal residual stress. It can be shown that the interfacial shear stress which is believed to play an important role in interfacial debonding was also much affected by the axial thermal residual stress in the bonded region. In Fig. 3(a) and Fig. 3(b), the variation of interfacial shear stresses which is proportional to the rate change of axial fiber stress as in Eq. (2) has two peaks at the loaded end (or debond front) and the bottom free end. The distribution of the interfacial shear stress in the bonded region may suggest two-way debonding. Comparison of the curves in Fig. 3(a) shows that the axial thermal residual stress induced to relatively higher peak values of interfacial shear stress at loaded end and weaker peak values at bottom end. Although the peak values of interfacial shear stresses are dependent on the material combination of fiber and matrix, the phenomenon is not shown in earlier works and is left for future experimental verification. The axial thermal residual stress does not cause any difference in both axial fiber stress and interfacial shear stress in the debonded region (Fig. 2(c) and Fig. 3(c)).

The applied stress required for further debonding at the debond length l can be determined from the interfacial debonding criterion of Eq. (39). The effect of axial thermal residual stress on interfacial debonding is shown in Fig. 4. The debonding length increases stably with increasing applied stress except for the unstable region ($l > 0.86L$). The applied stress required for proceeding the debond of the interface is higher in the

presence of the axial thermal residual stress. This can be interpreted as a discouragement of interfacial debonding due to thermal residual stress in the axial direction.

4. Conclusions

An improved model considering the effects of thermal residual stresses in both radial and axial directions is presented for the single fiber pull-out test. Stress distributions in the bonded region are significantly affected by the presence of the axial thermal residual stress. The amount of axial fiber stress in bonded region decreases with the axial thermal residual stress. The distribution of the interfacial shear stress in the bonded region also suggests a possibility of two-way debonding. Thermal residual stresses also affect the interfacial debonding behavior. It is shown that larger applied stresses are required for further debonding at the given debond length in the presence of the axial thermal residual stresses.

Acknowledgements

This work was supported by grant No. 981-100324-2 from the Basic Research Program of the Korea Science & Engineering Foundation (KOSEF) and was partly supported by the Brain Korea 21 Project in 2001.

References

Carter, W. C., Butler, E. P., and Fuller, E. R., 1991, "Micro-Mechanical Aspects of Asperity-Controlled Friction in Fiber-Toughened Ceramic Composites," *Scripta Metallurgica et Materialia*, Vol. 25, pp. 579~584

Gao, Y. C., Mai, Y. -W., and Cotterell B., 1988, "Fracture of Fiber-Reinforced Materials," *Journal of Applied Mathematics and Physics*, Vol. 39, pp. 550~558

Hutchinson, J. W., and Jensen, H. M., 1990, "Models of Fiber Debonding and Pullout in Brittle Composites with Friction," *Mechanics of Materials*, Vol. 9, pp. 139~163

Jero, P. D., and Kerans, R. J., 1991, "The Contribution of Interfacial Roughness to Sliding Friction of Ceramic Fiber in a Glass Matrix," *Scripta Metallurgica et Materialia*, Vol. 24, pp. 2315~2318

Kerans, R. J., and Parthasarathy, T. A., 1991, "Theoretical Analysis of the Fiber Pullout and Pushout Tests," *Journal of American Ceramic Society*, Vol. 74, pp. 1585~1596

Liu, H. Y., Zhou, L. M., and Mai, Y. -W., 1994, "On Fiber Pull-Out with a Rough Interface," *Philosophical Magazine*, Vol. 70, pp. 359~372

Liu, H. Y., Zhou, L. M., and Mai, Y. -W., 1995, "Effect of Interface Roughness on Fiber Push-Out Stress," *Journal of American Ceramic Society*, Vol. 78, pp. 560~566

Mackin, T. J., Yang, J., and Warren, P. D., 1992, "Influence of Fiber Roughness on the Sliding Behavior of Sapphire Fiber in TiAl and Glass Matrices," *Journal of American Ceramic Society*, Vol. 75, pp. 3358~3362

Mackin, T. J., Warren, P. D., and Evans, A. G., 1992, "Effect of Fiber Roughness on Interface Sliding in Composites," *Acta Metallurgica et Materialia*, Vol. 40, pp. 1251~1257

Parthasarathy, T. A., Marshall, D. B., and Kerans, R. J., 1994, "Analysis of the Effect of Interfacial Roughness on Fiber Debonding and Sliding in Brittle Matrix Composites," *Acta Metallurgica et Materialia*, Vol. 42, pp. 3773~3784

Parthasarathy, T. A., Barlage, D. R., Jero, P. D., and Kerans, R. J., 1994, "Effect of Interfacial Roughness Parameters on Fiber Pushout Behavior of a Model," *Journal of American Ceramic Society*, Vol. 77, pp. 3232~3236

Stukiewicz, S., 1996, "Fiber Sliding Model Accounting for Interfacial Micro-Dilatancy," *Mechancis of Materials*, Vol. 22, pp. 65~84

Zhou, L. M., and Mai, Y. -W., 1993, "A New Model for Evaluation of the Interfacial Frictional Coefficient and Residual Clamping Stress in a Fiber Push-Out Test," *Philosophical Magazine Letters*, Vol. 68, pp. 5~11

Zhou, L. M., and Mai, Y. -W., 1993, "On the Single Fiber Pullout and Pushout Problem : Effect of Fiber Anisotropy," *Journal of Applied*

Mathematics and Physics, Vol. 44, pp. 769~775

Zhou, L. M., Kim, J. K., Baillie, C., and Mai, Y. -W., 1995, "Fracture Mechanics Analysis of the Fibre Fragmentation Test," *Journal of Composite Materials*, Vol. 29, pp. 881~902

Appendix

$$m_1=(1-2\eta_2+2\eta_2^2)\frac{\partial F_1}{\partial l}+\eta_2(1-\eta_2)\frac{\partial F_2}{\partial l}+(1-2\eta_2)\,b_3\frac{\partial F_3}{\partial l}+\frac{\pi a^2}{2E_m}\alpha$$

$$m_2=\lambda\omega e^{\lambda t}[2(-1+\eta_2)F_1-(\eta_2F_2+b_3F_3)]+\omega(e^{\lambda t}-1)\left[2(-1+\eta_2)\frac{\partial F_1}{\partial l}-(\eta_2\frac{\partial F_2}{\partial l}+b_3\frac{\partial F_3}{\partial l})-\frac{\pi a^2}{E_m}\alpha\right]$$

$$m_3=\omega^2e^{2\lambda t}\left[(1-e^{-\lambda t})^2(\frac{\partial F_1}{\partial l}+b_2)+b_1\lambda^2+b_5k_1^2-2\lambda(1-e^{-\lambda t})F_1\right]$$

$$m_4=\left\{(1-2\eta_2)\left[-2\frac{\partial F_1}{\partial l}+\frac{\partial F_2}{\partial l}+2b_2\frac{\partial F_3}{\partial l}\right]+b_3\left[2\frac{\partial F_3}{\partial l}+1\right]\right\}\sigma_r$$

$$m_5=\lambda\omega e^{\lambda t}[2F_1-F_2-2b_2F_3]\sigma_r+\omega(e^{\lambda t}-1)\left[2\frac{\partial F_1}{\partial l}-\frac{\partial F_2}{\partial l}-2b_2\frac{\partial F_3}{\partial l}\right]\sigma_r$$

$$m_6=\left[2\frac{\partial F_1}{\partial l}-\frac{\partial F_2}{\partial l}-4b_2\frac{\partial F_3}{\partial l}-b_2\right]\sigma_r^2$$

where

$$F_1=\frac{1}{2\sqrt{\eta_1}}\left[(b_1\eta_1-b_2)\frac{\phi}{\sinh^2\phi}+(b_1\eta_1+b_2)\coth\phi\right]$$

$$F_2=\frac{1}{\sqrt{\eta_1}}\left[(b_1\eta_1-b_2)\frac{\phi\cosh\phi}{\sinh^2\phi}+(b_1\eta_1+b_2)\frac{1}{\sinh\phi}\right]$$

$$F_3=\frac{1}{\sqrt{\eta_1}}\frac{(1-\cosh\phi)}{\sinh\phi}$$

$$b_1=\frac{\pi(1+\nu_m)}{2E_m}\gamma^2\left[b^4\ln\frac{b}{a}-\frac{1}{4}(3b^2-a^2)(b^2-a^2)\right]$$

$$b_2=\frac{\pi a^2}{2E_m}(\alpha+\gamma)$$

$$b_3=\frac{\pi a^2}{E_m}[\gamma-(\alpha+\gamma)\eta_2]$$

$$b_4=\frac{\pi a^2}{2E_m}[\alpha\eta_2^2+\gamma(1-\eta_2)^2]$$

$$\phi=\sqrt{\eta_1}(L-l)$$

and

$$\bar{m}_1=m_1-m_2+m_3$$
$$\bar{m}_2=m_2-2m_3$$
$$\bar{m}_3=m_4-m_5$$
$$\bar{m}_4=m_2^2-4m_1m_3$$
$$\bar{m}_5=2m_4(m_2-2m_3)+2m_5(m_2-2m_1)$$
$$\bar{m}_6=(m_4-m_5)^2-4m_6(m_1-m_2+m_3)$$